Climate Dynamics Preceding Summer Forest Fires in California and the Extreme Case of 2018

TESS W. P. JACOBSON,[a,b] RICHARD SEAGER,[a] A. PARK WILLIAMS,[c] AND NAOMI HENDERSON[a]

[a] *Lamont-Doherty Earth Observatory, Palisades, New York*
[b] *Department of Earth and Environmental Sciences, Columbia University, New York, New York*
[c] *Department of Geography, University of California, Los Angeles, Los Angeles, California*

(Manuscript received 8 October 2021, in final form 2 March 2022)

ABSTRACT: Recent record-breaking wildfire seasons in California prompt an investigation into the climate patterns that typically precede anomalous summer burned forest area. Using burned-area data from the U.S. Forest Service's Monitoring Trends in Burn Severity (MTBS) product and climate data from the fifth major global reanalysis produced by the European Centre for Medium-Range Weather Forecasts (ERA5) over 1984–2018, relationships between the interannual variability of antecedent climate anomalies and July California burned area are spatially and temporally characterized. Lag correlations show that antecedent high vapor pressure deficit (VPD), high temperatures, frequent extreme high temperature days, low precipitation, high subsidence, high geopotential height, low soil moisture, and low snowpack and snowmelt anomalies all correlate significantly with July California burned area as far back as the January before the fire season. Seasonal regression maps indicate that a global midlatitude atmospheric wave train in late winter is associated with anomalous July California burned area. July 2018, a year with especially high burned area, was to some extent consistent with the general patterns revealed by the regressions: low winter precipitation and high spring VPD preceded the extreme burned area. However, geopotential height anomaly patterns were distinct from those in the regressions. Extreme July heat likely contributed to the extent of the fires ignited that month, even though extreme July temperatures do not historically significantly correlate with July burned area. While the 2018 antecedent climate conditions were typical of a high-burned-area year, they were not extreme, demonstrating the likely limits of statistical prediction of extreme fire seasons and the need for individual case studies of extreme years.

SIGNIFICANCE STATEMENT: The purpose of this study is to identify the local and global climate patterns in the preceding seasons that influence how the burned summer forest area in California varies year-to-year. We find that a dry atmosphere, high temperatures, dry soils, less snowpack, low precipitation, subsiding air, and high pressure centered west of California all correlate significantly with large summer burned area as far back as the preceding January. These climate anomalies occur as part of a hemispheric scale pattern with weak connections to the tropical Pacific Ocean. We also describe the climate anomalies preceding the extreme and record-breaking burned-area year of 2018, and how these compared with the more general patterns found. These results give important insight into how well and how early it might be possible to predict the severity of an upcoming summer wildfire season in California.

KEYWORDS: Atmosphere–land interaction; Climate variability; Forest fires; Hydrologic cycle; North America; Wildfires

1. Introduction

As a natural part of the coupling between climate and vegetation ecosystems, widespread wildfires have occurred for as long as Earth's atmosphere has contained sufficient oxygen to support burning and the land surface has had sufficient fuel load from vegetation (~350 million years ago) (Scott and Glasspool 2006). Historically, when humans move into a fire ecosystem, we influence that region's fire regime: in the western United States, this began as precolonial indigenous people controlling fires locally and igniting fires for management of the land (Anderson 2006; van Wagtendonk 2007). When European colonizers decimated the Native population, began logging forests and tilling grasslands, and brought livestock to graze, the vegetation and fire regime in the west were altered significantly. In the early twentieth century, the U.S. Forest Service (USFS) set out to completely suppress all fires on USFS land (Marlon et al. 2012; van Wagtendonk 2007). This suppression has allowed for the accumulation of fuel load in regions where fires were heavily suppressed such that a "fire deficit" has developed in these regions, and burned area is thus less constrained by fuel amount (Marlon et al. 2012; Williams et al. 2019). Additionally, the dramatic increase in burned area in the western United States over the latter half of the twentieth century has been confidently linked to increased aridity and reduced summer soil moisture, in part due to anthropogenic warming (Williams et al. 2019; Abatzoglou and Williams 2016; Westerling et al. 2006; Holden et al. 2018).

In addition to the increase in burned area over recent decades in the western United States, there is strong year-to-year variability in wildfire activity, and California's more severe wildfire seasons in particular have achieved widespread notoriety due to the death and destruction they have effected in

Corresponding author: Tess W. P. Jacobson, tessj@ldeo.columbia.edu

DOI: 10.1175/JAMC-D-21-0198.1

recent years, as well as their deleterious effect on air quality in the state (Phuleria et al. 2005; Wegesser et al. 2009; Shi et al. 2019). The 2018 wildfire season in California was devastating and record-breaking by measure of deaths, burned area, and structures destroyed (CALFIRE 2021; Herring et al. 2020). This was followed by the relatively quiet 2019 fire season, and then 2020, another record-setting fire season that burned almost 4% of the state (Higuera and Abatzoglou 2021). 2021 was yet another extreme wildfire season for California, with total burned area exceeding that of the 2018 season (CALFIRE 2021). Such extreme and destructive wildfire seasons prompt a diagnosis of the possible drivers in previous months and seasons of the interannual variability of California burned area. In this study we focus on this interannual variability, which is likely connected to regional- and hemispheric-scale climate variability and influenced by variability in the preceding summer, spring, and, possibly, winter.

Previous studies have found relationships between burned area in the western United States and local antecedent in situ climate variables such as soil moisture, vapor pressure deficit (VPD) and precipitation (Abatzoglou and Kolden 2013; Westerling et al. 2003; Crimmins and Comrie 2004; Williams et al. 2015). In this study, we go further to explore the relationships between summer California burned forest area variability and variability in atmospheric circulation and sea surface temperatures and examine the roles of these drivers in one particularly destructive fire season. While several variables exist for evaluating operational fire risk on synoptic scales, such as the Fosberg fire weather index (Fosberg 1978) and 1000-h fuel moisture (Cohen and Deeming 1985), our purpose is to relate summer burned forest area with antecedent atmospheric conditions on a seasonal and interannual basis. Hence, we focus primarily on monthly and seasonal anomalies in common atmospheric and hydrological predictors of forest fire in this region. In particular, we use VPD rather than operational fire risk variables because on interannual time scales, summer burned area in California has been found to correlate better with VPD than other integrative moisture-balance metrics (Williams et al. 2019). Similarly, Williams et al. (2014) studied the large-scale climate conditions that caused the extreme atmospheric aridity linked to the extreme 2011 wildfire season in the southwestern United States. The causes of the extreme 2018 wildfire season in California deserve such an investigation.

The fire season in California typically runs from May through November, and burned forest area reaches a maximum for fires ignited in July and August (Fig. 1). Summer fires in California are often enabled by fuel supply and atmospheric moisture deficits and are thus more susceptible to the climate conditions in antecedent months than fall fires. Wildfires in autumn are often driven by extreme offshore wind events, such as the Santa Ana winds that bring dry air downslope, westward and southward, from the Transverse and Peninsular Ranges. These winds can promote the rapid spread of existing wildfires (Williams et al. 2019; Westerling et al. 2003; Keeley and Fotheringham 2001). The yearly burned forest area by fires ignited in July have a large amount of year-to-year variability and July of 2018 was extreme in comparison with all previous Julys since at least 1984 (Fig. 2). Precipitation deficits and atmospheric aridity are also more influential on summer fire extent in forested ecosystems than nonforest ecosystems (Abatzoglou and Kolden 2013; Williams et al. 2019). 79% of summer fires from 1992 to 2018[1] in California were nonforest fires, whereas about 49% of burned area was nonforest. In the summer season of 2018, 78% of fires were nonforest, while only 31% of burned area was nonforest. Specifically, for fires ignited in July 2018, 74% of fires were nonforest and 35% of burned area was nonforest. Additionally, the percentage of California summer burned area occurring in forested regions has increased significantly in recent decades (Williams et al. 2019). Thus, in this study we characterize the antecedent sequences of climate anomalies that are robustly linked to California burned forest area in July and compare these sequences with the climate conditions leading up to the extreme fire season of 2018.

2. Data and methods

a. *Burned forest area and lightning data*

The burned-area data used are from the U.S. Forest Service's Monitoring Trends in Burn Severity (MTBS) product (Finco et al. 2012), reprocessed onto monthly 1 km × 1 km grid cells, for the period 1984–2018. Burned area in the MTBS product is for all land surface types, and for the monthly grids, the burned area is assigned to the month during which the fire attributed to that burn began. The MTBS product contains fires >404 ha, and fires classified as "prescribed" are excluded from the dataset. We approximate a monthly burned forest area time series by multiplying the burned area in each grid cell by the forest-cover fraction in that cell. The forest-cover fractions are calculated from the National Land Cover Database (NLCD) (Homer et al. 2012). The NLCD produced eight land-cover products from 1992 to 2016, from which we produced 1-km grids of forest fractional cover. We then make a single map of forest fraction by assigning to each grid cell the maximum forest fraction value among the eight versions of the dataset, because this is most likely to best represent prefire forest coverage in each grid cell. For all analyses, the burned forest area is summed over all California grid cells to create a time series of monthly total burned forest area in California. We chose to work with burned-area data directly, rather than the logarithm of burned area as in Williams et al. (2019), because both the distributions of July California burned forest area and logarithm of July California burned forest area are relatively normal (with respective skews of 2.5 and −2.5 and kurtoses of 8.2 and 9.8 after detrending), and the resulting correlation coefficients in section 3 are stronger using burned forest area than the logarithm of burned forest area.

For analyses of lightning and human ignition events and other background information on individual fires, we also use the dataset of western U.S. fires from Short (2017), which

[1] Summer is defined as May–September, and here we use the dataset of individual fires from Short (2017).

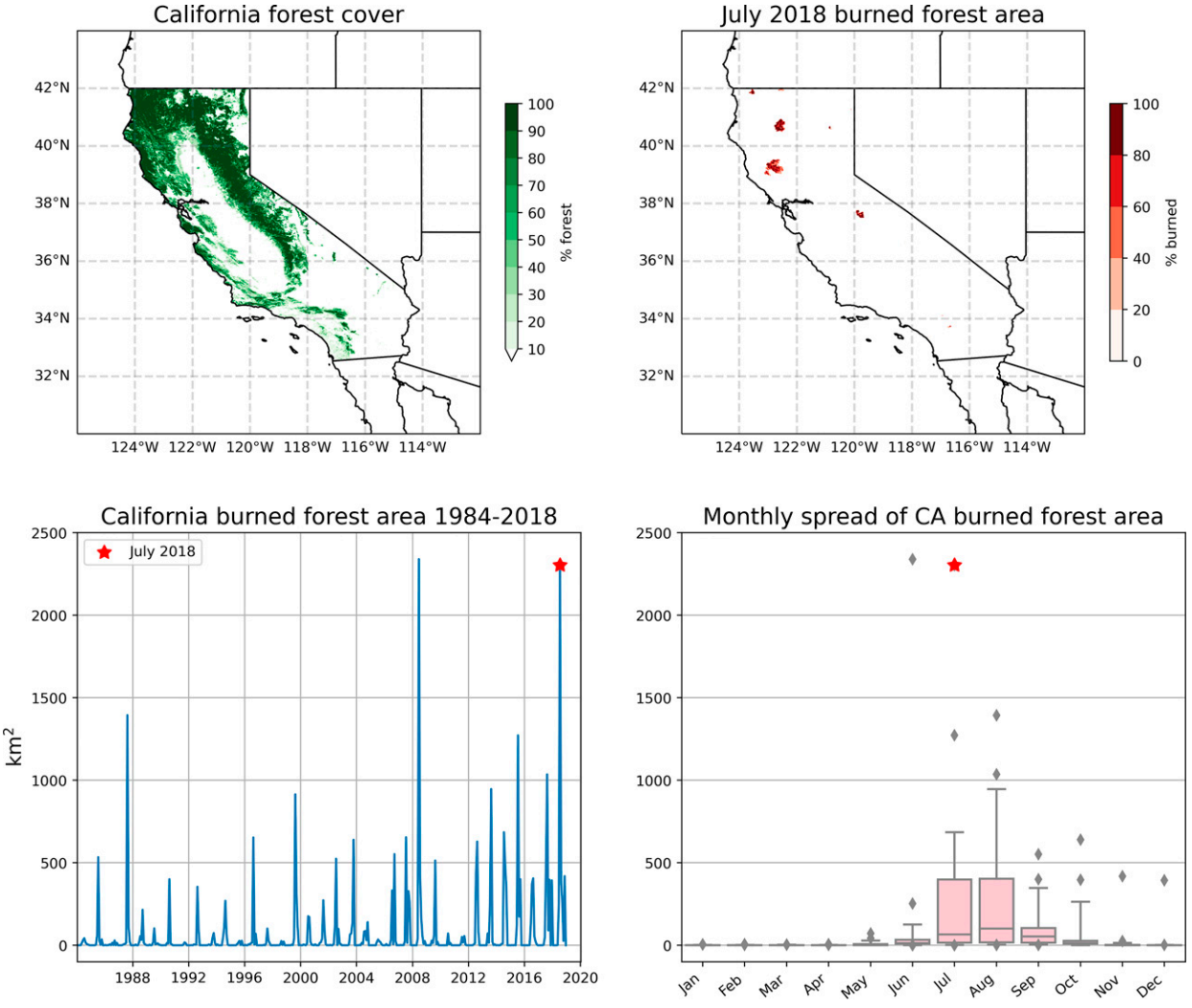

FIG. 1. (top left) Percent forest cover in California, (top right) burned forest area in California for fires ignited in July 2018 as percent of 1-km^2 grid cells burned, (bottom left) monthly time series of burned forest area in California 1984–2018 (km^2), and (bottom right) boxplot of the monthly distribution of California burned forest area over 1984–2018, with boxes indicating the interquartile range, whiskers at the 5th and 95th percentiles, and gray diamonds showing outliers. July 2018 is indicated in the bottom two plots with a red star.

contains individual fires ranging down to as small as 0.1 acre (1 acre = 0.4 ha). Burned forest area for this dataset is estimated by treating each fire as a circle centered over the latitude and longitude provided and overlaying the circle on a map of NLCD forest fraction. Forest fires are then defined as fires with ≥50% of the total burned area in a forested region. We also use a dataset of lightning strike density from the National Lightning Detection Network, which we reprocessed onto monthly 12 km × 12 km grid cells.

b. *Climate data*

For the climate and surface hydrology data in this study, we use the fifth major global reanalysis produced by European Centre for Medium-Range Weather Forecasts (ECMWF) (ERA5) for the 1984–2018 period, gridded at 0.25° resolution (Hersbach et al. 2020). We chose to use an atmospheric reanalysis product for this study because reanalyses connect surface climate variables with atmospheric circulation and ocean variables in a dynamically consistent manner. We use ERA5 in particular because it is a recently released, state-of-the-art atmospheric reanalysis product with higher spatial resolution than prior reanalyses. To validate our choice of ERA5 we reran the lag correlation analysis in section 3 using the Gridded Surface Meteorological (gridMET) temperature and precipitation dataset of Abatzoglou (2013), which combines surface observations with the North American Land Data Assimilation System Phase 2 (NLDAS-2) regional reanalysis (Mitchell et al. 2004) and found results consistent with ERA5. For brevity, we do not include these results in this paper. Unless otherwise specified, we accessed all fields at a monthly temporal resolution. In addition, we use the hourly minimum and maximum 2-m temperature to

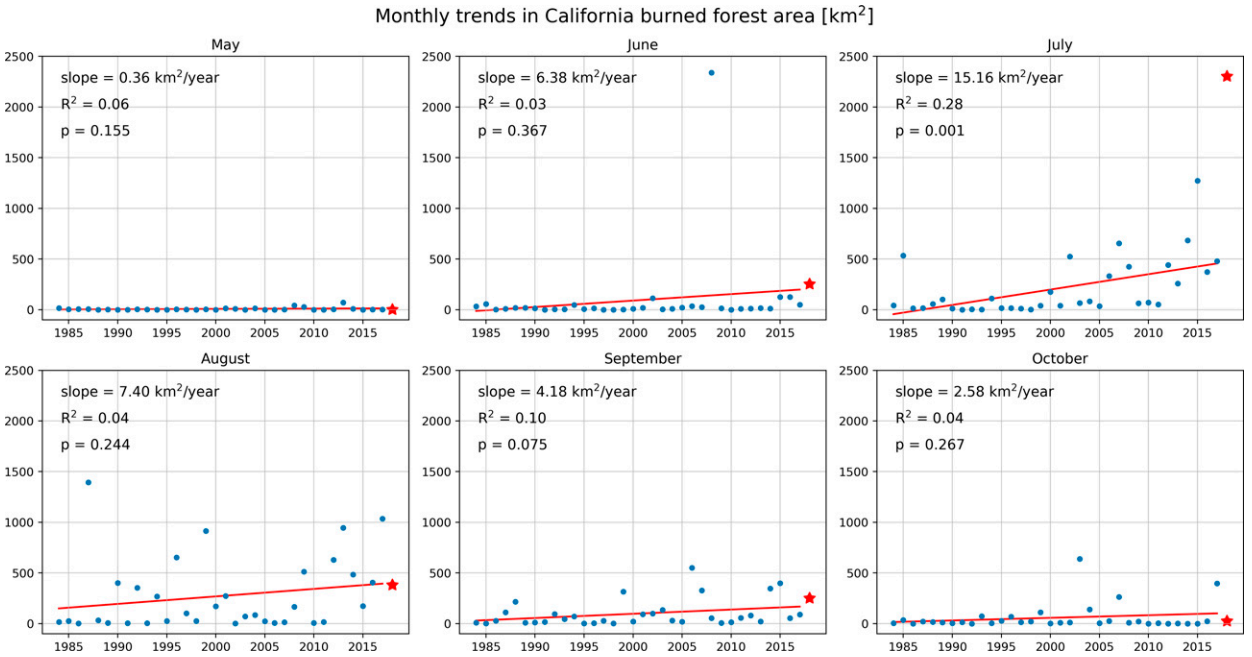

FIG. 2. Linear trends in California burned forest area for the months of May–October. In each panel, burned forest area for the respective month of each year is plotted in blue, with the trend line calculated over the 1984–2017 period shown in red, and the 2018 burn for that month plotted as a red star. Slope, R^2, and p value for Student's t test with a two-sided null hypothesis are shown in each panel for the linear regression over the 1984–2017 period.

calculate the daily minimum and maximum 2-m temperature, and hourly 2-m temperature and dewpoint temperature to calculate the daily minimum and maximum vapor pressure deficit. We calculate VPD, a measure of atmospheric aridity that is the difference between saturation vapor pressure and actual vapor pressure, as in Seager et al. (2015b).

To calculate daily maximum (and minimum) 2-m temperatures and VPD, we take the maximum (minimum) of the hourly data for each day. Then, to quantify the frequency of extreme temperatures, which is an important metric in addition to monthly mean temperatures because it can capture heat wave frequency, we create a monthly time series for the number of days in each month that have a daily maximum temperature greater than the 75th percentile of daily maximum temperatures for that day of the year over the 1984–2018 period. We repeat this for high daily minimum temperatures and maximum and minimum VPD, and for the 90th percentile threshold as well.

c. *Lag correlations and regressions*

To quantify which climate variables affect July burned forest area and during which months, we perform a lag correlation analysis with monthly resolution. Climate anomalies are calculated for each grid point as deviations from the monthly climatology over the period 1979–2017. Then, the linear trend over the period is removed from both the July California burned forest area time series and the California-averaged anomalies in order to remove any contribution to the correlations due to common long-term trends rather than year-to-year variability. The lag correlations are calculated as the correlation coefficients between the detrended July California burned forest area time series and the detrended California-averaged anomalies of climate variables in months around the summer fire season, from the previous November to the following October. The year 2018 is excluded from correlation analysis in order to describe the relationships between burned forest area and climate up until the extreme year of 2018 and avoid biasing the results by the extreme conditions in 2018.

Similarly, to make maps of the climate conditions associated with large July burned forest area in seasons preceding July ignition, we take the January–March (JFM) and April–June (AMJ) climate anomalies during 1984–2017. Then, we detrend these anomalies and for each grid point calculate their linear regression slopes with the detrended July California burned forest area time series and plot these regression coefficients.

3. Climate anomalies associated with anomalous California July burned forest area

Figure 3 shows the lag correlation coefficients with burned forest area for anomalous California-averaged VPD, 2-m temperature, specific humidity, precipitation, vertical wind at 700 hPa, and number of days with daily T_{max} and daily T_{min} higher than the 90th percentile, and anomalous geopotential height at 500 hPa averaged over a box west of the coast in the North Pacific Ocean, from 30° to 50°N and 120° to 150°W. The 95% significance threshold is shown as a pink dashed line.

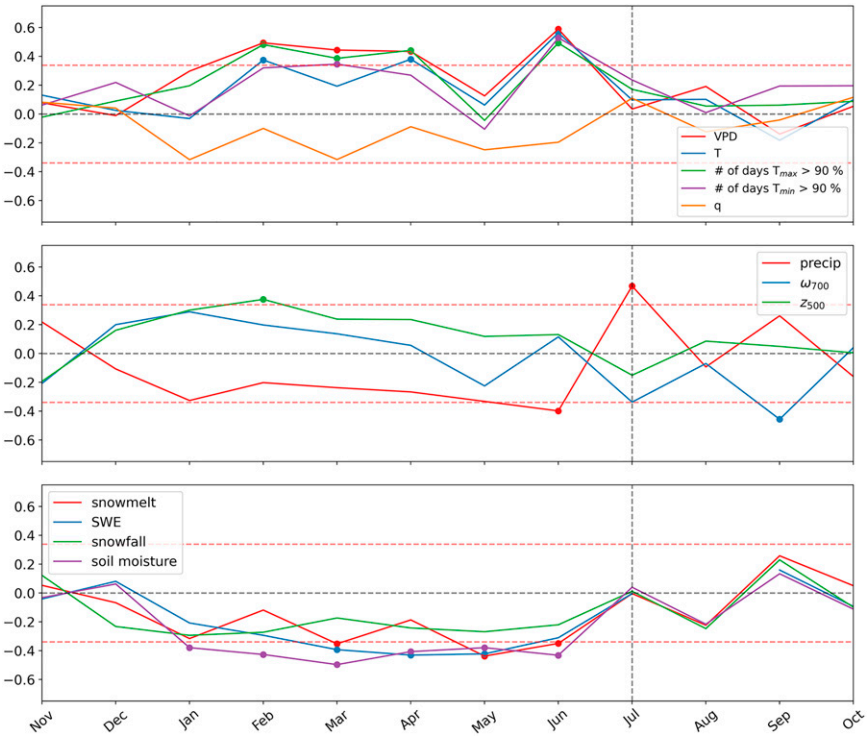

FIG. 3. Correlation coefficients of detrended July California burned forest area with detrended climate anomalies in the preceding November through the following October. Correlations are calculated using 1984–2017 data. Pink dashed lines indicate the 95% significance threshold, and months for which the correlation is significant above this threshold are marked with a circle. July is marked with a vertical dashed line. (top) Correlation coefficients for VPD, 2-m temperature T, number of days in the month with maximum daily temperature greater than the 90th percentile for that day (No. of days $T_{max} > 90\%$), number of days in the month with minimum daily temperature greater than the 90th percentile for that day (No. of days $T_{min} > 90\%$), and specific humidity q. (middle) Correlation coefficients for precipitation (precip), subsidence at 700 hPa ω_{700}, and geopotential height anomaly at 500 hPa z_{700}. (bottom) Correlation coefficients for snowmelt, SWE, snowfall, and 0–7-cm soil moisture. All fields are averaged over all of California except geopotential height z_{500}, which is averaged over the 30°–50°N, 120°–150°W box.

The lag correlations r for VPD, temperature, and frequency of T_{max} extremes with July burned forest area are generally positive in preceding months and closely track each other, while humidity correlation coefficients are negative from January through June and are not statistically significant. Of all variables in all months, June VPD has the strongest correlation with July burned forest area at nearly $r \sim 0.6$. VPD and extreme T_{max} frequency in the preceding February through April are also significantly correlated with July burned forest area, and the correlation coefficient drops off in months before February and after July. The correlation coefficients for temperature follow a similar pattern but are generally weaker during February–June and are not significant in March. Extreme T_{min} frequency only correlates significantly with July burned forest area in March and June. July VPD, temperature, extreme T_{min} and T_{max} frequency, and humidity do not correlate significantly with July burned forest area, implying that the antecedent atmospheric aridity and temperature conditions in June and before are statistically more important to the amount of burned forest area from fires ignited in July than the July conditions themselves.

Curiously, July burned forest area is correlated with increased precipitation and upward motion. Although we do not show results from this analysis here, this is likely due to precipitation associated with the July storms that contribute to lightning-ignited fires. Both lightning strikes and convective available potential energy (CAPE), a proxy for lightning (Romps et al. 2014), in California have a climatological peak across July and August. Similar to precipitation, July CAPE correlates significantly ($r = 0.35$) with July burned forest area, and also with July lightning strikes ($r = 0.64$). Using the dataset of Short (2017), which provides ignition classifications for fires ranging as small as 0.1 ha, we find that the number of lightning-ignited fires in July correlates with July precipitation with $r = 0.43$. The correlation between July precipitation and lightning-ignited burned forest area is strongly positive as well ($r = 0.64$) but is seemingly driven by a single year with

anomalously high precipitation and lightning-ignited burned forest area (2015). Human-ignited burned forest area in July does not significantly correlate with July precipitation. Thus, we suggest that the link between positive precipitation anomaly and burned forest area in July reflects the effect of lightning ignitions from thunderstorms that also cause anomalous precipitation. However, further investigation beyond the scope of this study is required to confirm this supposal.

Precipitation correlates negatively with July burned forest area for the months before July, starting in January, with local extrema for its negative correlation in January and June. Additionally, a ridge off of the West Coast at 500 hPa averaged over 30°–50°N and 120°–150°W positively correlates with July burned forest area during the preceding December—June, and the correlation coefficient is significant in February.

These lag correlations are mostly consistent with the intuitive notion that large burns that begin in July are preceded by drier and hotter conditions than usual. The land surface correlations provide some insight into the mechanisms behind these relationships. Top layer (0–7 cm) soil moisture is significantly negatively correlated with July burned forest area from the January through June before the fire year. From March through May, snow water equivalent (SWE) correlates negatively and significantly with July burned forest area, as does snowmelt in March, April, and June. Snowfall never significantly correlates with July burned forest area but maintains a negative correlation from December through June. These correlations suggest that low soil moisture in the winter and spring, which could be caused by less precipitation during the winter wet season or more sublimation and less snowmelt, is linked to high burned forest area in the summer. This is logical as low soil moisture can desiccate vegetation, making fuels easier to burn. Also, dry soils can contribute to land surface feedbacks whereby low soil moisture increases evaporative demand, driving up surface temperatures and VPD (Seneviratne et al. 2010). Then, high VPD in late winter and spring can draw moisture out of soils and vegetation further, setting the system up for high burned area. Additionally, less snow mass and snowmelt in the spring can dry out the vegetation that relies on snowmelt for moisture after the winter. Thus, the land surface, circulation, and thermodynamic processes that affect summer fire are all highly interrelated and sensitive to year-to-year variability in these variables. An important finding is that none of the months before January have significant correlations between variable anomalies and July burned forest area, suggesting that it is the late winter, spring, and summer climate conditions that most influence summer burned forest area in California.[2]

Since June VPD has the strongest correlation with July burned forest area, it is useful to see which fields vary with June VPD concurrently and in preceding months (Fig. 4). June precipitation has the highest magnitude correlation with June VPD at $r \sim -0.8$, and May precipitation has the next highest, with

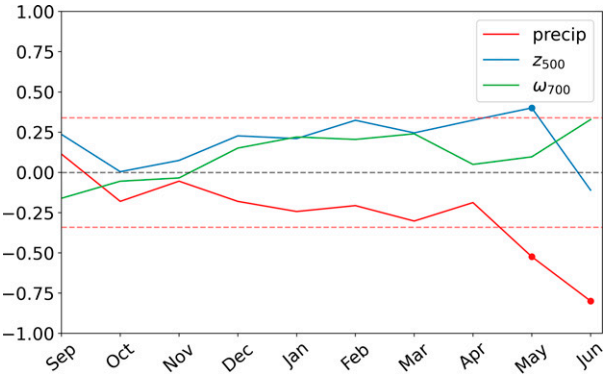

FIG. 4. Correlation coefficients of California-averaged detrended June VPD with preceding September–June California-averaged detrended anomalous precipitation, 30°–50°N and 120°–150°W geopotential height at 500 hPa z_{500}, and California-averaged subsidence at 700 hPa from 1984 to 2017 ω_{700}. Pink dashed lines indicate the 95% significance threshold, and months for which the correlation is significant above this threshold are marked with a circle.

precipitation in April and earlier dropping off and not significantly correlated with June VPD. Although subsidence in California is never significantly correlated with June VPD, it does maintain a generally positive correlation as far back as the previous December. Geopotential height in the North Pacific region is positively and significantly correlated with June VPD in May and weakly negatively correlated in June. The subsidence and height relations are consistent with the idea that an offshore high pressure system with northerly subsiding flow and suppressed precipitation over California favors high VPD. Therefore, June VPD, which has the strongest correlation with July burned forest area, varies with May and June precipitation and May geopotential height off the West Coast.

The relations shown so far make clear that, despite significance levels varying month to month, high July burned forest area is favored by high pressure, subsidence, low precipitation, high VPD, low soil moisture, low snowpack and snowmelt, and high surface air temperature from the preceding late winter through to early summer. The thermodynamic variations are themselves consistent with the large-scale circulation anomalies. Hence, next we look at the spatial patterns of the governing climate and circulation anomalies. Given that climate anomalies as early as January correlate significantly with July burned forest area, the monthly climate anomalies are averaged over JFM and AMJ to only include the months before the July fires begin. These seasonal anomalies are then detrended and linearly regressed onto the detrended California burned forest area. The regression slopes are plotted as maps in Figs. 5 and 6, with colors only shown where significant at the 95% confidence level for Fig. 5 and the 90% level for Fig. 6.

In the preceding winter (JFM), high July burned forest area in California is typically associated with a ridge off the West Coast and anomalously low precipitation in California and over the ocean off the coast of California. Anomalously dry

[2] Using climate anomalies averaged over northern California where the large majority of July 2018 burned area occurred, instead of over the entire state, does not noticeably change the results in Fig. 3.

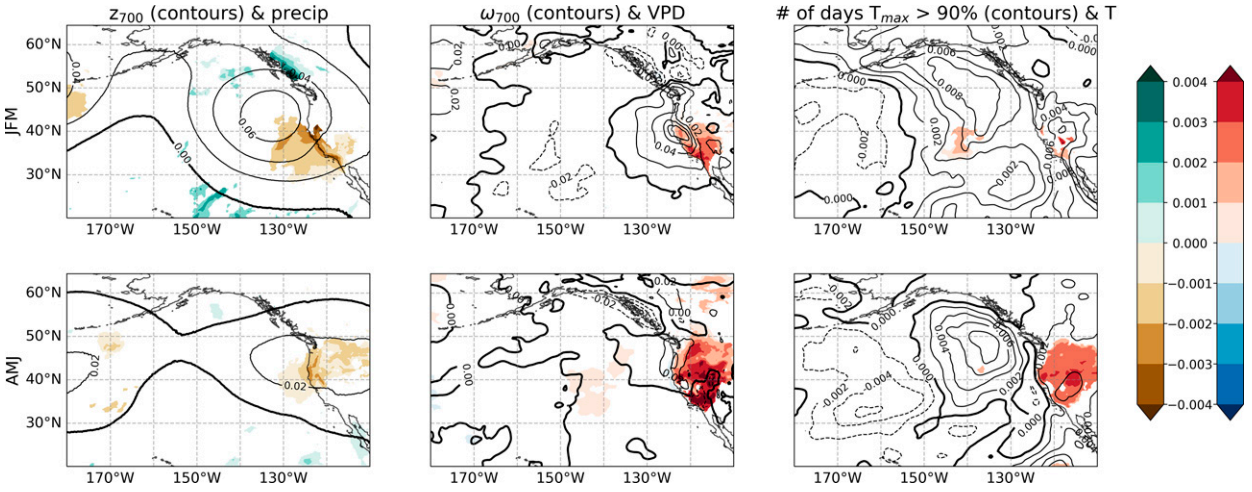

FIG. 5. Regression coefficients for detrended July California burned forest area with detrended seasonal climate anomalies over 1984–2017. Regression coefficient at each grid point using (top) JFM and (bottom) AMJ seasonal averages, showing (left) regression coefficients for geopotential height at 700 hPa z_{700} in contours and precipitation in color shading, (center) regression coefficients for subsidence at 700 hPa ω_{700} in contours and VPD in color shading, and (right) regression coefficients for the average number of days per month with maximum daily temperature greater than the 90th percentile for that day (No. of days $T_{max} > 90\%$) in contours and 2-m temperature T in color shading. Contours for subsidence and number of extreme temperature days are smoothed with a 0.75° rolling mean in longitude and latitude. Colors are shown only where the regression coefficient is greater than the 95% significance threshold, and the units of the regression coefficient are unit per kilometer squared, where the units are meters for geopotential height, millimeters per day for precipitation, pascals per second for subsidence, hectopascals for VPD, days per month for $T_{max} > 90\%$, and kelvin for temperature.

surface air, subsidence, high surface temperature, and more frequent T_{max} extremes in JFM, particularly in Southern California, are also significantly associated with subsequent high burned forest area.

In the preceding spring (AMJ), there is also a ridge at 500 hPa associated with high burned forest area, centered over California and the West Coast of the United States. Dry and hot spring conditions in California—anomalously low precipitation, high VPD, high surface temperature, and more frequent extreme T_{max} days—are also typical of years with high burned forest area in July. The regression coefficients for VPD are larger in spring than in winter, meaning that high local VPD in the preceding spring has a more pronounced relationship with summer California burned forest area than high VPD in the preceding winter. Precipitation in California, however, has larger regression coefficients in the preceding winter than the preceding spring, perhaps related to more climatological precipitation in the winter than in the spring. In addition, winters with low precipitation contribute to high VPD in the summer by drying out soils, which can cause surface temperature in following months to increase due to a decrease in evapotranspiration, which increases sensible heating and VPD (Seneviratne et al. 2010; Seager et al. 2015b).

To put these local climate patterns into a larger climate dynamics perspective, Fig. 6 shows regression coefficients for geopotential height at 200 and 700 hPa, sea surface temperature (SST), and precipitation on a global scale. The offshore winter ridge in Fig. 5 is part of a circumglobal atmospheric wave train with wavenumber 4, and the cyclone pair straddling the equator in the east Pacific are characteristic of La Niña conditions. However, the La Niña relation must be weak because it is not seen as statistically significant in the SSTs. La Niña–like precipitation patterns over the Pacific are also typical of the winter before a large July burned forest area season. In AMJ, there is still a circumglobal Rossby wave train, but it is weaker and any connection to the tropics is gone. The strong correlation with large-scale geopotential height patterns, including the high off the coast and lack of strong correlations with SSTs, is consistent with the idea that California hydroclimate is primarily affected by internal atmospheric variability, and only secondarily affected by ENSO, especially in northern California where most burned forest area occurs (Williams et al. 2021; Baek et al. 2021; Seager et al. 2015a).

4. Climate anomalies in 2018 and diagnosing causes of extreme burned forest area

Having characterized the climate anomalies associated with anomalous July burned forest area in California, we move on to examine the climate anomalies in the months preceding July 2018, an extreme burned forest area year. Figure 7 shows the same anomalies that were regressed on burned forest area but for JFM and AMJ of 2018. In the 2018 winter, there was a ridge offshore, but centered around 165°W and 50°N, slightly to the north and west of the ridge that appears in the regressions. There was widespread anomalous subsidence on the eastern flank of this ridge including over California. This led to anomalously high VPD in winter connected to circulation around the ridge bringing northerly, subsiding flow to California. The winter subsidence went along with

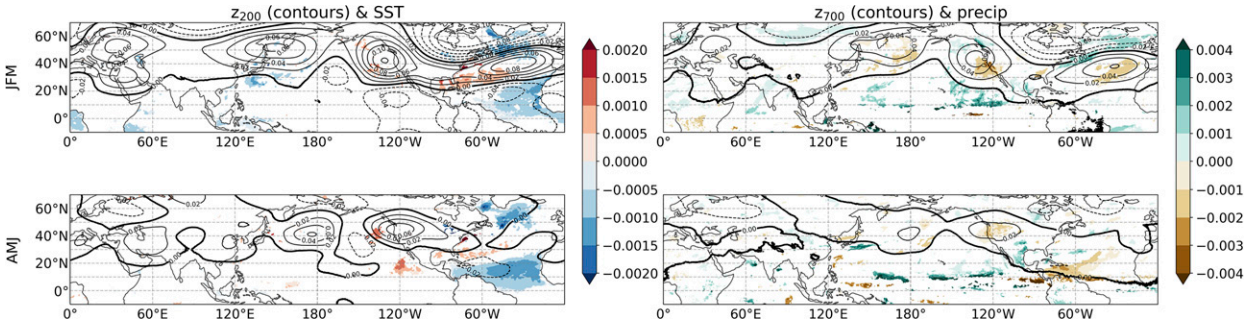

FIG. 6. As in Fig. 5, but showing regressions of detrended July California burned forest area with detrended (left) geopotential height at 200 hPa z_{200} in contours and SST in color shading and (right) geopotential height at 700 hPa z_{700} in contours and precipitation in color shading. Colors are shown where the regression coefficient is greater than the 90% significance threshold. Units are the same as Fig. 5 for geopotential height and precip, and units for the SST regression plot are kelvins per kilometer squared.

anomalously low precipitation in Northern California; however, the precipitation anomaly was not more than 1 standard deviation away from the mean in California, so it does not appear in Fig. 7. There were also high surface temperature anomalies in the southwest, both for monthly mean temperature and extreme temperature days in winter 2018. In the spring of 2018, there was a weak high over the West Coast of the United States and a very large VPD anomaly in the southwest that went along with high temperatures and more extreme hot days.

Figure 8 shows the global-scale seasonal anomalies in 2018 for geopotential height at 200 and 700 hPa, SST, and precipitation. The winter 2017–18 La Niña is evident in both SST and precipitation patterns, and the winter 200-hPa geopotential height anomaly is that of the normal negative mode of the Pacific–North American (PNA) pattern, which is typically associated with La Niña winters (Seager et al. 2014). In addition, there is a suggestion of a Rossby wave train over the North Atlantic. The spring anomalies are approximately a muted version of the winter anomalies associated with La Niña, typical of the weakening of tropical–extratropical teleconnections in the transition from boreal winter to summer as the mean flow weakens (Webster 1982; Kumar and Hoerling 1998).

Thus, the climate conditions in the six months before the extreme forest fire ignitions in July 2018 were as follows: a La Niña winter in 2017–18 induced a Rossby wave train propagating across the PNA region that included a high in the North Pacific, west of the West Coast of North America (Fig. 8). This high caused dry, but not significantly dry, precipitation conditions in California in the winter, along with subsidence in Northern California, high VPD and high temperatures across the southwest. In the spring, there was a much weaker wave train with a high over the West Coast and very high VPD and temperature anomalies in the southwest. These conditions differ slightly from the typical patterns found in Figs. 5 and 6 to precede large July burned forest areas, in the structure of the winter Rossby wave train and thus the location of the offshore high, as well as the lack of significant precipitation anomalies in both the winter and spring and the lack of a subsidence anomaly in the spring. However, in both the regressions and in the 2018 anomalies we see the importance of subsidence, high VPD, and high

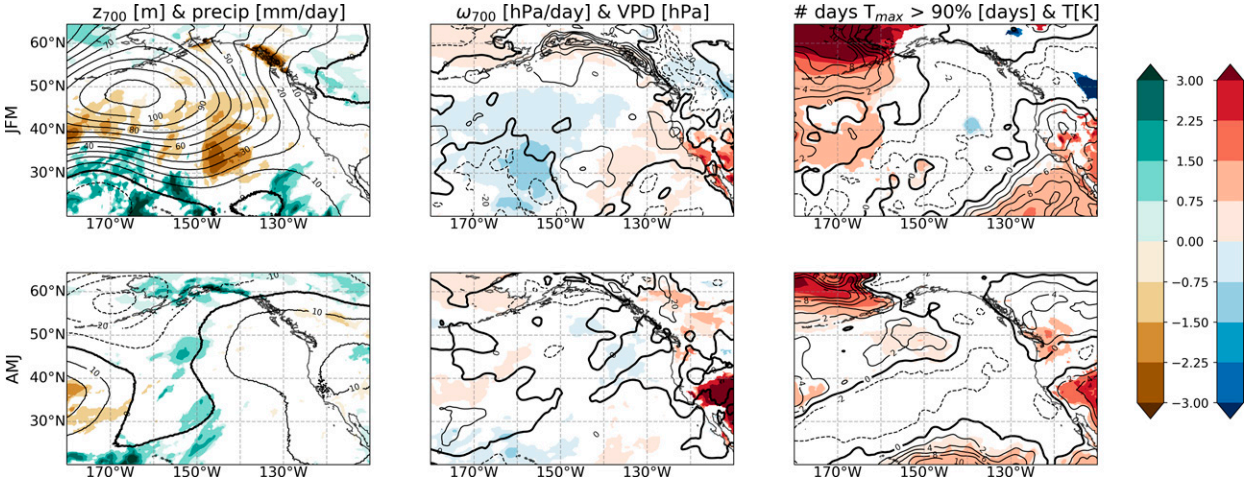

FIG. 7. As in Fig. 5, but instead of regression coefficients, showing seasonal anomalies in 2018.

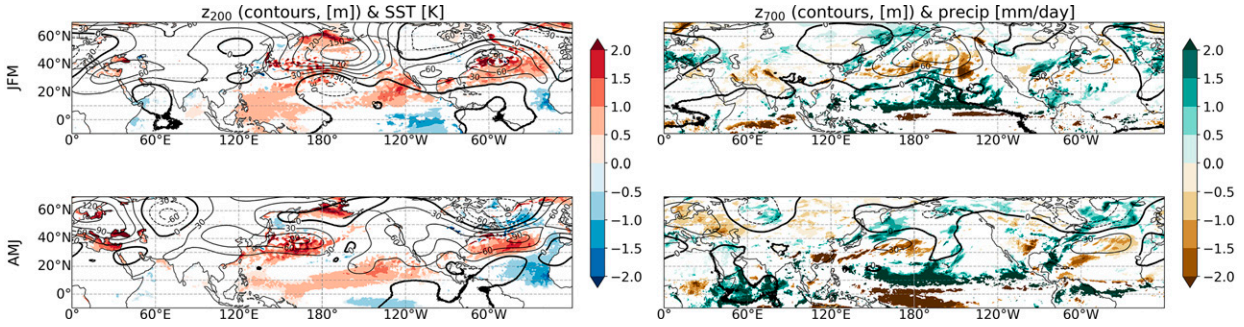

FIG. 8. As in Fig. 6, but instead of regression coefficients, showing seasonal anomalies in 2018.

surface temperatures over the preceding half-year in setting up for high burned forest area in the summer.

While the 2018 antecedent climate conditions in many ways resemble the regressions, 2018 does not appear to be particularly extreme in the history of California-averaged climate anomalies. For example, while both June VPD and January precipitation correlate with burned forest area (with $r = 0.59$ and 0.33, respectively), 2018 had high but not extreme VPD in June and low but not extreme precipitation in January (Fig. 9, left). On the other hand, snowmelt anomalies in May and June were indeed the lowest on record but by a minute margin (on the order of thousandths of millimeters per day) (Fig. 9, right), whereas statewide soil moisture and snow water equivalent were anomalously low in January through June of 2018 but not extreme (not shown). The hydrological conditions in the first half of 2018 were typical of a larger-than-average fire season, however, they were not so extreme to statistically predict that July 2018 would have the most extensive July burned forest area in the 35-yr record by almost twofold. Other factors must have contributed to the extremeness of July 2018.

Even though the California-averaged number of extreme T_{min} and T_{max} days per month in July or August did not correlate strongly with burned forest area in July over the analysis period, California did experience extreme heat in July 2018 and, to some extent, August 2018 that likely contributed to the spread of the fires ignited in July. Figure 10 shows the distribution of California-averaged daily maximum and minimum 2-m temperatures and VPDs for each day in July over the 1984–2018 period, as well as the values for each day of July 2018. Of the 31 days in July 2018, 28 had a hotter average maximum and minimum temperature than the median temperature for that day over the period. Further, daily minimum temperatures were consistently above the 75th percentile from the 6th day of the month onward. High daily minimum temperatures can promote the spread of fire by slowing fire containment efforts and drying out fuels by reducing overnight humidity recovery (Herring et al. 2020; Chiodi et al. 2021; Balch et al. 2022). The daily maximum VPD in July 2018 followed the daily maximum temperature in pattern, with three peaks separated by about 10 days each. However, unlike the daily minimum temperature, the daily minimum VPDs in July 2018 were not consistently in the upper daily quartile, but instead followed the variations in daily maximum temperature.

While it is useful to look at this day-by-day development of July 2018 in comparison with the other Julys in the period, spatially averaging the temperature and VPD metrics over all of California could mask localized extremes in the regions where the large forest fires in July 2018 occurred (see Fig. 1). The three largest fires in Fig. 1 made up 90% of the burned forest area in California in July 2018. From north to south, the

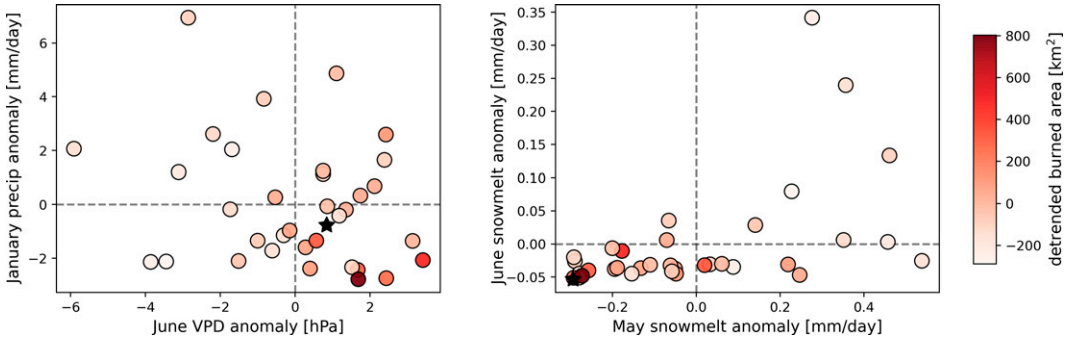

FIG. 9. (left) Detrended June California-averaged VPD anomaly (hPa; x axis) and detrended January California-averaged precipitation anomaly (mm day^{-1}; y axis) for each year 1984–2018, detrended using the 1984–2017 trend. (right) Detrended May (x axis) and June (y axis) California-averaged snowmelt anomaly (mm day^{-1}); 2018 is plotted as a black star, and the circles are colored by the detrended burned forest area in July of that year (km^2).

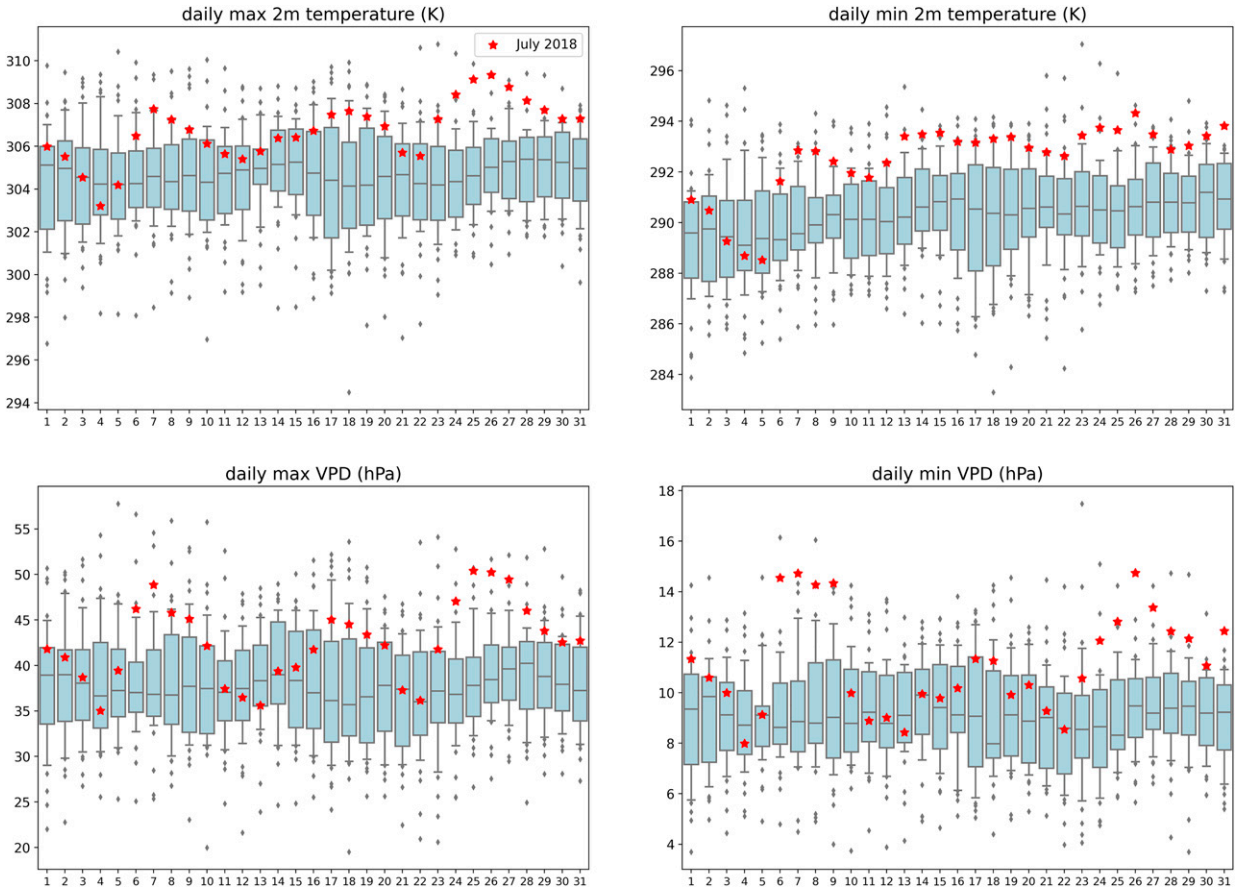

FIG. 10. July distribution of (top left) daily maximum 2-m temperature (K), (top right) daily minimum 2-m temperature (K), (bottom left) daily maximum VPD (hPa), and (bottom right) daily minimum VPD for 1984–2018. The boxes indicate the middle quartiles of the data, and the whiskers extend to the 10th and 90th percentiles, with outliers plotted as diamonds. Each day of July 2018 is shown as a red star.

fires shown are the Carr Fire (712 km^2 of burned forest area), the Mendocino Complex Fire (1054 km^2 of burned forest area), and the Ferguson Fire (305 km^2 of burned forest area).

To examine the spatial patterns of extremes in July 2018 we calculated for each July over 1984–2018 and each point in California the number of extreme (>75th and 90th percentile for that day) July days for daily maximum and minimum temperature and VPD. We then determined where July 2018 ranked in this distribution. The ranks are plotted in Fig. 11 along with the location of the three largest fires that contributed 90% to the total burned forest area from July 2018. In most of central California, and all of the regions with fire except for a small corner of the Carr Fire, July 2018 had the most days with 75th percentile daily minimum surface temperature of any July in the analysis period. For days in the 75th percentile daily maximum surface temperature, July 2018 is similarly extreme in most of the fire region, except it does not definitively rank the highest. In terms of VPD, in most of the fire regions, July 2018 consistently ranks in the top half of years for number of days with extreme daily maximum and minimum VPD and ranks the highest just to the east of the Mendocino Complex Fire. The rankings for number of extreme temperature and VPD days in the 90th percentile are, in general, lower than those for the 75th-percentile threshold; however, there are still large swaths of the state where July 2018 had the most days with extreme minimum and maximum temperature. In the fire regions the 90th-percentile minimum and maximum temperature days in 2018 consistently rank in the top half. The 90th-percentile minimum and maximum VPD days vary in rank throughout the state and do not have the top rank anywhere in the fire regions.

Averaged over all of California, of all Julys 1984–2018, July 2018 had the most days[3] with 75th percentile daily minimum and daily maximum temperatures and 90th percentile daily minimum temperatures and was second in number of days with 90th-percentile daily maximum temperatures (Fig. 12). In a similar way, July 2018 had anomalous daily minimum and

[3] July 2015 is the other extreme burned forest area that appears as a very dark red dot in Figs. 9 and 12. In Fig. 9, July 2015 was preceded by the driest January over the 1984–2018 period and a high, but not extremely high, June VPD anomaly, as well as anomalously low snowmelt in May and June. In Fig. 12, July 2015 actually had few extreme daily minimum and maximum temperature and VPD days, except for daily maximum temperature days in the 90th percentile, of which July 2015 had a small positive anomaly.

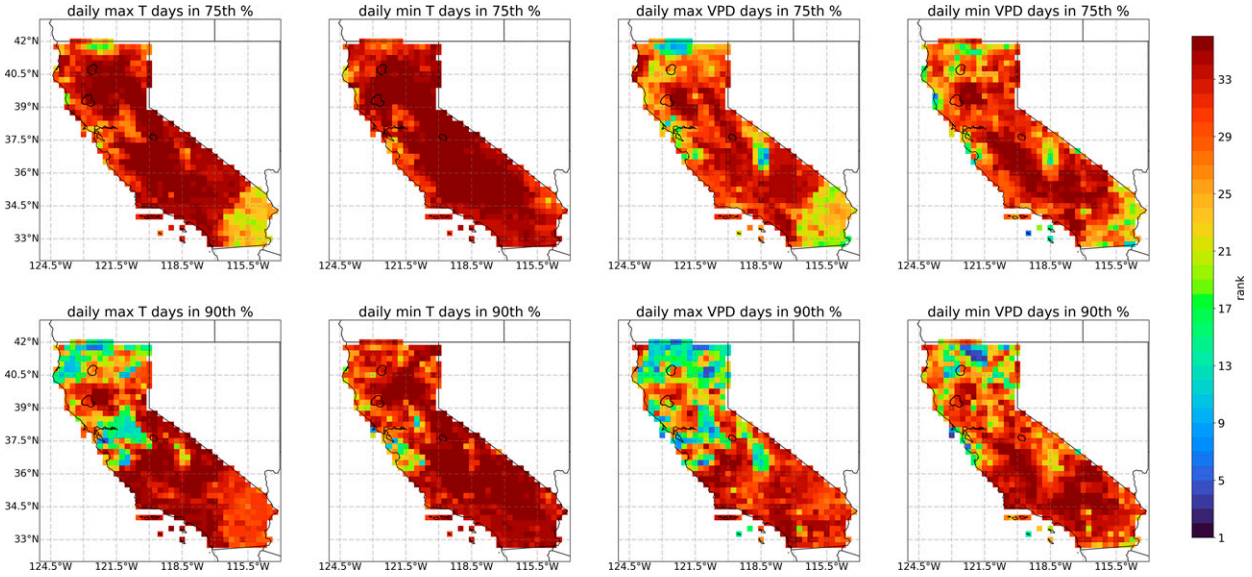

FIG. 11. Rank of July 2018, in comparison with Julys 1984–2018, in terms of the number of days in the (top) 75th and (bottom) 90th percentile for that day of daily (left) maximum 2-m temperatures, (left center) minimum 2-m temperatures, (right center) maximum VPD, and (right) minimum VPD. Data are ranked in descending order, with dark red representing areas where July 2018 had the most number of days with the given variable in the given percentile, in comparison with all other Julys in the period. Locations of the three largest fires in July 2018 are enclosed in black contours.

maximum VPD days for both the 75th- and 90th-percentile thresholds, but was not the most extreme in this regard. However, the relationship of these metrics with July burned forest area in general is not strong, as evidenced by the lack of a visible relationship with burned forest area (scatter colors in Fig. 12) as well as by the low correlation coefficients in Fig. 3. Figures 10–12 show that July 2018 was extreme in terms of days with high daily maximum and minimum surface temperatures, particularly daily minimums, and that these extremes were, in some regions, accompanied by extremes in the number of days with high minimum and maximum VPD.

While here we focused on the case study of temperature and VPD extremes in July 2018, note that the large fires ignited in July 2018 were not contained until mid-August–September, and so similar hot and dry conditions in August 2018 likely promoted the extreme burned forest area of the July 2018 fires. The equivalent analysis for extreme minimum and maximum temperatures and VPD days in August 2018 revealed that August 2018 was anomalously hot and dry in California but not extreme relative to other Augusts in terms of the number of extremely hot and dry days. Still, the temperature and VPD conditions in August 2018 likely enabled the continued spread of July-ignited fires.

5. Conclusions and discussion

We found that monthly climate anomalies as early as the January before the fire season correlate significantly with July burned forest area in California over the 1984–2017 period. In particular, anomalously low precipitation, increased subsidence, an offshore ridge, and high VPD and surface temperatures in the preceding winter all correlate strongly with anomalous burned forest area. In the preceding spring, high VPD, a high over the West Coast of the United States, high temperatures, increased frequency of extreme temperature days, and low precipitation correlate with large July burned forest area. These local relationships are part of a larger regression pattern including La Niña–like precipitation and height anomalies in the North Pacific and a circumglobal Rossby wave train with wavenumber 4 in winter and 5 in spring. The bridging across seasons which allows winter climate anomalies to impact fire in summer is provided by snow mass and soil moisture. Reduced rain directly reduces soil moisture while reduced winter and spring snow will introduce a lag until reduced snowmelt in late spring dries soils directly ahead of the fire season. Aided by reduced snow mass and precipitation in winter and spring, high temperatures and VPD dry vegetation and soils, favoring greater burned forest area in July.

Climate anomalies in the winter and spring of 2018 preceding the extreme July burned forest area in some ways matched these regression patterns. The winter and spring were hot and dry, but more significant in Southern California and the southwest, and precipitation anomalies were negative but not significant. Winter 2017–18 was a La Niña winter, and there was a Rossby wave train with a negative PNA pattern typical of La Niña winters, with a ridge centered farther north and west of the ridge in the regressions. While the antecedent climate conditions were close to those found for high burned forest area years in general, the atmospheric anomalies that usually correlate with July burned forest area, such as winter precipitation and July VPD, were not extreme enough in 2018 to explain the record-setting burned forest area of July 2018. Snow hydrology variables that typically vary with July burned forest area in

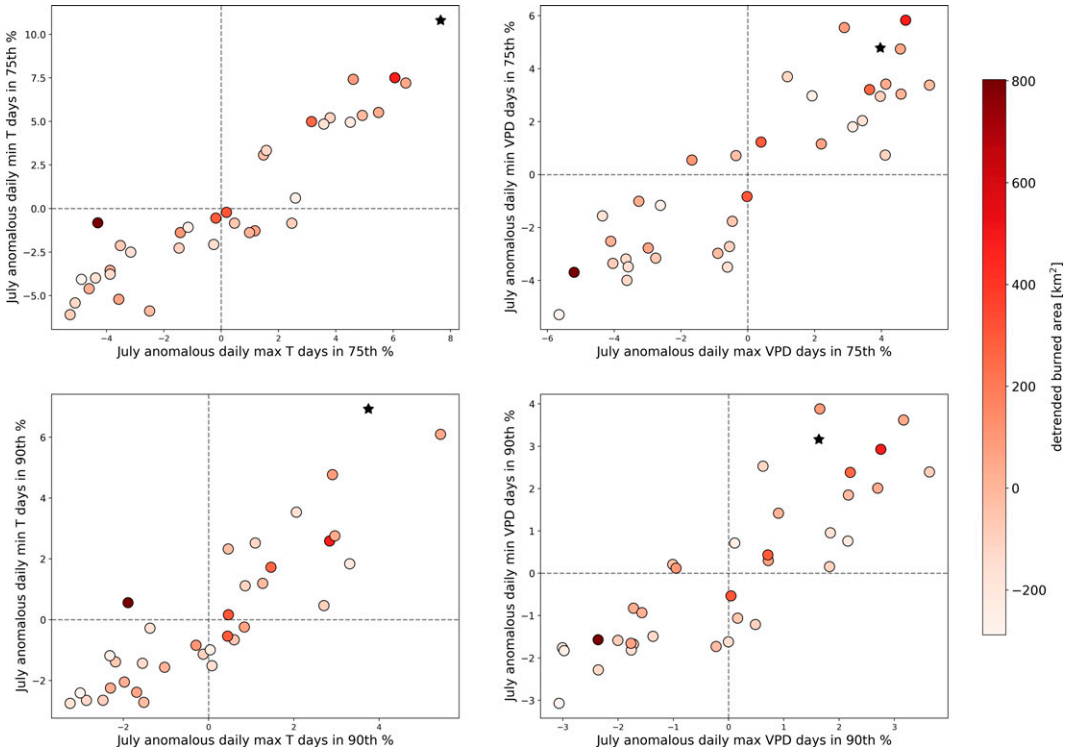

FIG. 12. Detrended July California-averaged anomalous number of days in the (top) 75th and (bottom) 90th percentile for that day of daily (left) maximum and minimum 2-m temperatures and (right) maximum and minimum VPD for each year 1984–2018, detrended using the 1984–2017 trend; 2018 is plotted as a black star. The circles are colored by the detrended burned forest area in July of that year (km^2).

winter and spring, such as snowmelt and soil moisture, were anomalously low in 2018. Only late spring snowmelt was extreme in 2018, and only narrowly so, such that it was unlikely to be the main cause of extreme burned area in July. Rather, we found that even though July California surface temperatures and the number of extremely high minimum and maximum temperature days do not typically correlate with July burned forest area, extreme surface temperatures and particularly many extremely high overnight low temperatures were likely a factor in the record-setting burned forest area in July 2018. Nighttime temperatures can have a critical influence on fire suppression and spread. While it is well known that high daytime temperatures can exacerbate the spread of wildfires (Abatzoglou and Williams 2016; Abatzoglou et al. 2019), Balch et al. (2022) found that overnight low temperatures are a particularly important barrier to fire spread and that hotter and drier nighttime conditions are linked with increased nighttime fire intensity.

While the statistical relationships between antecedent climate anomalies and July burned forest area are robust for many variables, this case study of summer 2018 California fires shows the likely limits of these statistical relationships in predicting individual extremes. The climate conditions evolving in the first six months of 2018 were similar to what we would expect of a year with anomalously high July burned forest area, and these conditions likely enabled high burned forest area by drying out fuels. However, without predicting the meteorological factors such as the local extreme heat in the fire regions in July 2018, we would not have been able to predict the record-breaking burned forest area of the July 2018 fires. Forest fires require an ignition event by lightning or humans, and the proper fuel conditions, and even then, burned forest area is sensitive to day-to-day weather and suppression efforts. Since our statistical analysis of antecedent climate conditions does not account for all of these factors that affect forest fires, we expect there to be a limit to the predictability of extreme fire seasons using antecedent climate. It might have been expected that extreme burned forest area in a July would arise from equally extreme antecedent climate anomalies but for 2018 this was not the case. Instead, it appears the antecedent climate anomalies set the stage but then extreme daily maxima and minima temperatures and VPD in July 2018 itself turned what would have been a high burned forest area July into a record extreme one.

The differential anomalies in climate conditions and burned forest area in 2018 may also be evidence of the emerging possibility of record-shattering burned area during conditions of anomalous but not record-shattering heat and drought due to the observed exponential response of burned forest area to VPD (Williams et al. 2019; Juang et al. 2022). This exponential response implies that with background warming, the interannual variability in burned forest area will increase even if the

interannual variability in climate anomalies does not, allowing for such extreme fire years as 2018, 2020, and 2021 (Abatzoglou et al. 2019). Our analysis quantifies the linear relationships between burned forest area and antecedent climate, which we found captured stronger lag correlations for the 1984–2017 period than exponential relationships using logarithm of burned area. However, because the above work has established exponential relationships between seasonal and annual burned area and VPD, it is possible that the extreme burned forest areas of 2018, 2020, and 2021 are harbingers of emerging extraordinary increases in burned area with more moderate increases in heat and drought conditions.

Characterizing the climate factors and their timing that influence the interannual variability of California wildfires is crucial to our understanding of the predictability of large and devastating wildfire years. While the 2018 wildfire season in California was by many metrics the worst on record at the time, the 2020 wildfire season broke records yet again, with the so-called August Complex Fire, which burned from August to November 2020, surpassing the Mendocino Complex Fire to become the largest California wildfire. In 2021, the Dixie Fire had greater burned area than the Mendocino Complex Fire and is the largest single noncomplex fire on record (CALFIRE 2021). Many recent studies have examined the role of anthropogenic climate change and warming-driven atmospheric changes in this increased wildfire activity in the west (Williams et al. 2019; Abatzoglou and Williams 2016; Kirchmeier-Young et al. 2019; Goss et al. 2020; Westerling et al. 2006; Westerling 2016, 2018). Still, with increased wildfire activity there is year-to-year variability, and our ability to diagnose the large-scale antecedent climate conditions that enable anomalous burned area is becoming increasingly relevant as the extreme years become more and more extreme. In addition, with background warming and changes in the seasonal cycles of precipitation in the western United States, an important extension of the findings of this study would be to explore potential shifts in the statistical relationship between summer burned forest area and antecedent climate conditions due to warming-induced changes.

Acknowledgments. This research was supported by Columbia University's Graduate School of Arts and Sciences, the National Science Foundation Graduate Research Fellowship Program, National Oceanic and Atmospheric Administration Awards NA20OAR4310379 and NA20OAR4310425, National Science Foundation Award NSFAGS2127684, U.S. Department of Energy Office of Science Award DE-SC-0022302, and a grant from the Zegar Family Foundation. In addition, we thank Caroline Juang for contributing to discussions about the burned-area data.

Data availability statement. The ERA5 data used in this study are freely available from the ECMWF website (https://www.ecmwf.int/en/forecasts/datasets/reanalysis-datasets/era5). The MTBS burned-area and NLCD forest-cover datasets are available online (https://www.mtbs.gov/ and https://www.mrlc.gov/data, respectively). Karen Short's database of individual fires with ignition cause is available online (https://www.fs.usda.gov/rds/archive/Catalog/RDS-2013-0009.5). Lightning strike density data are available from the National Lightning Detection Network (https://www1.ncdc.noaa.gov/pub/data/swdi/database-csv/v2/).

REFERENCES

Abatzoglou, J. T., 2013: Development of gridded surface meteorological data for ecological applications and modelling. *Int. J. Climatol.*, **33**, 121–131, https://doi.org/10.1002/joc.3413.

——, and C. A. Kolden, 2013: Relationships between climate and macroscale area burned in the western United States. *Int. J. Wildland Fire*, **22**, 1003–1020, https://doi.org/10.1071/WF13019.

——, and A. P. Williams, 2016: Impact of anthropogenic climate change on wildfire across western US forests. *Proc. Natl. Acad. Sci. USA*, **113**, 11 770–11 775, https://doi.org/10.1073/pnas.1607171113.

——, ——, and R. Barbero, 2019: Global emergence of anthropogenic climate change in fire weather indices. *Geophys. Res. Lett.*, **46**, 326–336, https://doi.org/10.1029/2018GL080959.

Anderson, M., 2006: The use of fire by Native Americans in California. *Fire in California's Ecosystems*, University of California Press, 417–430.

Baek, S. H., J. E. Smerdon, B. I. Cook, and A. P. Williams, 2021: U.S. Pacific coastal droughts are predominantly driven by internal atmospheric variability. *J. Climate*, **34**, 1947–1962, https://doi.org/10.1175/JCLI-D-20-0365.1.

Balch, J. K., J. T. Abatzoglou, M. B. Joseph, M. J. Koontz, A. L. Mahood, J. McGlinchy, M. E. Cattau, and A. P. Williams, 2022: Warming weakens the night-time barrier to global fire. *Nature*, **602**, 442–448, https://doi.org/10.1038/s41586-021-04325-1.

CALFIRE, 2021: CALFIRE. State of California, accessed 10 August 2021, http://www.fire.ca.gov/.

Chiodi, A. M., B. E. Potter, and N. K. Larkin, 2021: Multi-decadal change in western US nighttime vapor pressure deficit. *Geophys. Res. Lett.*, **48**, e2021GL092830, https://doi.org/10.1029/2021GL092830.

Cohen, J. D., and J. E. Deeming, 1985: The National Fire-Danger Rating System: Basic equations. USDA Forest Service Pacific Southwest Forest and Range Experiment Station General Tech. Rep. PSW-GTR-82, 16 pp., https://www.fs.fed.us/psw/publications/documents/psw_gtr082/psw_gtr082.pdf.

Crimmins, M. A., and A. C. Comrie, 2004: Interactions between antecedent climate and wildfire variability across south-eastern Arizona. *Int. J. Wildland Fire*, **13**, 455–466, https://doi.org/10.1071/WF03064.

Finco, M., B. Quayle, Y. Zhang, J. Lecker, K. A. Megown, and C. K. Brewer, 2012: Monitoring Trends and Burn Severity (MTBS): Monitoring wildfire activity for the past quarter century using Landsat data. *Moving from Status to Trends: Forest Inventory and Analysis Symp. 2012*, Baltimore, MD, USDA, 222–228, https://www.nrs.fs.fed.us/pubs/gtr/gtr-nrs-p-105papers/35finco-p-105.pdf.

Fosberg, M. A., 1978: Weather in wildland fire management: The fire weather index. *Conf. on Sierra Nevada Meteorology*, South Lake Tahoe, CA, Amer. Meteor. Soc., 1–4.

Goss, M., D. L. Swain, J. T. Abatzoglou, A. Sarhadi, C. A. Kolden, A. P. Williams, and N. S. Diffenbaugh, 2020: Climate change is increasing the likelihood of extreme autumn wildfire conditions across California. *Environ. Res. Lett.*, **15**, 094016, https://doi.org/10.1088/1748-9326/ab83a7.

Herring, S. C., N. Christidis, A. Hoell, M. P. Hoerling, and P. A. Stott, 2020: Explaining extreme events of 2018 from a climate perspective. *Bull. Amer. Meteor. Soc.*, **101** (1), S1–S140, https://doi.org/10.1175/BAMS-ExplainingExtremeEvents2018.1.

Hersbach, H., and Coauthors, 2020: The ERA5 global reanalysis. *Quart. J. Roy. Meteor. Soc.*, **146**, 1999–2049, https://doi.org/10.1002/qj.3803.

Higuera, P. E., and J. T. Abatzoglou, 2021: Record-setting climate enabled the extraordinary 2020 fire season in the western United States. *Global Change Biol.*, **27**, 1–2, https://doi.org/10.1111/gcb.15388.

Holden, Z. A., and Coauthors, 2018: Decreasing fire season precipitation increased recent western US forest wildfire activity. *Proc. Natl. Acad. Sci. USA*, **115**, E8349–E8357, https://doi.org/10.1073/pnas.1802316115.

Homer, C. H., J. A. Fry, and C. A. Barnes, 2012: The National Land Cover Database. U.S. Geological Survey Fact Sheet 2012-3020, 4 pp., https://pubs.usgs.gov/fs/2012/3020/fs2012-3020.pdf.

Juang, C. S., A. P. Williams, J. T. Abatzoglou, J. K. Balch, M. D. Hurteau, and M. A. Moritz, 2022: Rapid growth of large forest fires drives the exponential response of annual forest-fire area to aridity in the western United States. *Geophys. Res. Lett.*, **49**, e2021GL097131, https://doi.org/10.1029/2021GL097131.

Keeley, J. E., and C. Fotheringham, 2001: Historic fire regime in Southern California shrublands. *Conserv. Biol.*, **15**, 1536–1548, https://doi.org/10.1046/j.1523-1739.2001.00097.x.

Kirchmeier-Young, M., N. Gillett, F. Zwiers, A. Cannon, and F. Anslow, 2019: Attribution of the influence of human-induced climate change on an extreme fire season. *Earth's Future*, **7**, 2–10, https://doi.org/10.1029/2018EF001050.

Kumar, A., and M. P. Hoerling, 1998: Annual cycle of Pacific–North American seasonal predictability associated with different phases of ENSO. *J. Climate*, **11**, 3295–3308, https://doi.org/10.1175/1520-0442(1998)011<3295:ACOPNA>2.0.CO;2.

Marlon, J. R., and Coauthors, 2012: Long-term perspective on wildfires in the western USA. *Proc. Natl. Acad. Sci. USA*, **109**, E535–E543, https://doi.org/10.1073/pnas.1112839109.

Mitchell, K. E., and Coauthors, 2004: The multi-institution North American Land Data Assimilation System (NLDAS): Utilizing multiple GCIP products and partners in a continental distributed hydrological modeling system. *J. Geophys. Res.*, **109**, D07S90, https://doi.org/10.1029/2003JD003823.

Phuleria, H. C., P. M. Fine, Y. Zhu, and C. Sioutas, 2005: Air quality impacts of the October 2003 Southern California wildfires. *J. Geophys. Res.*, **110**, D07S20, https://doi.org/10.1029/2004JD004626.

Romps, D. M., J. T. Seeley, D. Vollaro, and J. Molinari, 2014: Projected increase in lightning strikes in the United States due to global warming. *Science*, **346**, 851–854, https://doi.org/10.1126/science.1259100.

Scott, A. C., and I. J. Glasspool, 2006: The diversification of Paleozoic fire systems and fluctuations in atmospheric oxygen concentration. *Proc. Natl. Acad. Sci. USA*, **103**, 10 861–10 865, https://doi.org/10.1073/pnas.0604090103.

Seager, R., L. Goddard, J. Nakamura, N. Henderson, and D. E. Lee, 2014: Dynamical causes of the 2010/11 Texas–northern Mexico drought. *J. Hydrometeor.*, **15**, 39–68, https://doi.org/10.1175/JHM-D-13-024.1.

——, M. Hoerling, S. Schubert, H. Wang, B. Lyon, A. Kumar, J. Nakamura, and N. Henderson, 2015a: Causes of the 2011–14 California drought. *J. Climate*, **28**, 6997–7024, https://doi.org/10.1175/JCLI-D-14-00860.1.

——, A. Hooks, A. P. Williams, B. Cook, J. Nakamura, and N. Henderson, 2015b: Climatology, variability, and trends in the U.S. vapor pressure deficit, an important fire-related meteorological quantity. *J. Appl. Meteor. Climatol.*, **54**, 1121–1141, https://doi.org/10.1175/JAMC-D-14-0321.1.

Seneviratne, S. I., T. Corti, E. L. Davin, M. Hirschi, E. B. Jaeger, I. Lehner, B. Orlowsky, and A. J. Teuling, 2010: Investigating soil moisture–climate interactions in a changing climate: A review. *Earth-Sci. Rev.*, **99**, 125–161, https://doi.org/10.1016/j.earscirev.2010.02.004.

Shi, H., and Coauthors, 2019: Modeling study of the air quality impact of record-breaking Southern California wildfires in December 2017. *J. Geophys. Res. Atmos.*, **124**, 6554–6570, https://doi.org/10.1029/2019JD030472.

Short, K. C., 2017: Spatial wildfire occurrence data for the United States, 1992–2015 [FPA_FOD_20170508]. 4th ed. Forest Service Research Data Archive, accessed 11 February 2022, https://doi.org/10.2737/RDS-2013-0009.4.

van Wagtendonk, J. W., 2007: The history and evolution of wildland fire use. *Fire Ecol.*, **3**, 3–17, https://doi.org/10.4996/fireecology.0302003.

Webster, P. J., 1982: Seasonality in the local and remote atmospheric response to sea surface temperature anomalies. *J. Atmos. Sci.*, **39**, 41–52, https://doi.org/10.1175/1520-0469(1982)039<0041:SITLAR>2.0.CO;2.

Wegesser, T. C., K. E. Pinkerton, and J. A. Last, 2009: California wildfires of 2008: Coarse and fine particulate matter toxicity. *Environ. Health Perspect.*, **117**, 893–897, https://doi.org/10.1289/ehp.0800166.

Westerling, A. L., 2016: Increasing western US forest wildfire activity: Sensitivity to changes in the timing of spring. *Philos. Trans. Roy. Soc.*, **B371**, 20150178, https://doi.org/10.1098/rstb.2015.0178.

——, 2018: Wildfire simulations for California's Fourth Climate Change Assessment: Projecting changes in extreme wildfire events with a warming climate. California Energy Commission Sacramento Rep., 57 pp., https://www.energy.ca.gov/sites/default/files/2019-11/Projections_CCCA4-CEC-2018-014_ADA.pdf.

——, A. Gershunov, T. J. Brown, D. R. Cayan, and M. D. Dettinger, 2003: Climate and wildfire in the western United States. *Bull. Amer. Meteor. Soc.*, **84**, 595–604, https://doi.org/10.1175/BAMS-84-5-595.

——, H. G. Hidalgo, D. R. Cayan, and T. W. Swetnam, 2006: Warming and earlier spring increase western US forest wildfire activity. *Science*, **313**, 940–943, https://doi.org/10.1126/science.1128834.

Williams, A. P., and Coauthors, 2014: Causes and implications of extreme atmospheric moisture demand during the record-breaking 2011 wildfire season in the southwestern United States. *J. Appl. Meteor. Climatol.*, **53**, 2671–2684, https://doi.org/10.1175/JAMC-D-14-0053.1.

——, and Coauthors, 2015: Correlations between components of the water balance and burned area reveal new insights for predicting forest fire area in the southwest United States. *Int. J. Wildland Fire*, **24**, 14–26, https://doi.org/10.1071/WF14023.

——, J. T. Abatzoglou, A. Gershunov, J. Guzman-Morales, D. A. Bishop, J. K. Balch, and D. P. Lettenmaier, 2019: Observed impacts of anthropogenic climate change on wildfire in California. *Earth's Future*, **7**, 892–910, https://doi.org/10.1029/2019EF001210.

Williams, A., K. Anchukaitis, C. Woodhouse, D. Meko, B. Cook, K. Bolles, and E. Cook, 2021: Tree rings and observations suggest no stable cycles in Sierra Nevada cool-season precipitation. *Water Resour. Res.*, **57**, e2020WR028599, https://doi.org/10.1029/2020WR028599.